

Structure of $\text{Zn}_{1-x}\text{Mn}_x\text{In}_2\text{Se}_4$ crystals grown by CVT

J. Mantilla†, G. E. S. Brito†, E. ter Haar†, V. Sagredo‡, V. Bindilatti†§

† Instituto de Física, Universidade de São Paulo
Cx. Postal 66.318, 05315-970 S. Paulo, SP, Brazil

‡ Laboratorio de Magnetismo, Universidad de los Andes, Mérida 5101, Venezuela

Abstract. Single crystals of $\text{Zn}_{1-x}\text{Mn}_x\text{In}_2\text{Se}_4$ were grown by the chemical vapour phase transport (CVT) technique. Through X-rays powder diffraction patterns and Laue diagrams of single crystals we studied the transformation from the layered rhombohedral structure of MnIn_2Se_4 to the tetragonal structure of ZnIn_2Se_4 . On the ZnIn_2Se_4 side, we observe single-phase, solid solution samples for $x=0.01$ and $x=0.25$, as is the case for the MnIn_2Se_4 side with $x=1$ and $x=0.87$. For the intermediate concentrations $x=0.35$, $x=0.60$ and $x=0.67$ we observe our samples to be two-phase mixtures.

PACS numbers: 61.12.Ld, 71.20.Nr, 81.15.Kk

Submitted to: *J. Phys.: Condens. Matter*

1. Introduction

While much is known about II–VI diluted magnetic semiconductors (DMS) containing manganese[1], the structurally and magnetically more complex ternary and quaternary systems have recently begun to be studied[2], in the expectation of exploring and manipulating the interactions between the electronic, magnetic and structural degrees of freedom. An example is cation disorder, which can be studied by its effect on the magnetic properties[3, 4]. Spin-glass behaviour was observed in $\text{Zn}_{1-x}\text{Mn}_x\text{In}_2\text{Te}_4$ [5] and in MnIn_2Se_4 [6], end-point of the $\text{Zn}_{1-x}\text{Mn}_x\text{In}_2\text{Se}_4$ series we investigate here. The low Mn concentration side of the series is structurally similar to the II-VI DMS, in which extensive investigation of the exchange interactions between Mn^{2+} ions has been performed[7]. To extend these investigations to $\text{Zn}_{1-x}\text{Mn}_x\text{In}_2\text{Se}_4$, an important first question is for what substitution concentrations it is possible to obtain homogeneous solid solutions, since in this series the two endpoint compounds are in different crystal systems.

The structures of the ternary compounds of the II–III₂–VI₄ family (II: bivalent metal, III: trivalent metal and VI: chalcogen atom) are found in three major types: a cubic structure (spinel), a tetragonal defective zinc blende structure and a rhombohedral structure [8]. The latter two structures are realized by the end-points of the $\text{Zn}_{1-x}\text{Mn}_x\text{In}_2\text{Se}_4$ series.

§ E-mail: vbindilatti@if.usp.br

ZnIn_2Se_4 crystallizes in a tetragonal cell of space group $I\bar{4}2m$ with parameters $a=5.710 \text{ \AA}$ and $c=11.420 \text{ \AA}$. This structure is a defective chalcopyrite with the metal atoms randomly distributed within the cationic sub-lattice[9, 10]. MnIn_2Se_4 exhibits a rhombohedral structure with space group $R\bar{3}m$ and lattice constants $a=4.051 \text{ \AA}$ and $c=39.460 \text{ \AA}$. In this layered structure, the unit cell consists of three van der Waals coupled slabs, each slab consisting of four Se layers in the sequence $ABCA$. Between these layers there are octahedral and tetrahedral sites, which are again thought to be randomly filled by the Mn and In atoms[11, 12].

In this paper we report the growth of single crystals as well as the structural characterization of the $\text{Zn}_{1-x}\text{Mn}_x\text{In}_2\text{Se}_4$ series. We used X-ray techniques to study the transformation from the tetragonal structure of ZnIn_2Se_4 to the rhombohedral structure of MnIn_2Se_4 .

2. Experimental

2.1. Sample preparation

Single crystals of $\text{Zn}_{1-x}\text{Mn}_x\text{In}_2\text{Se}_4$ with nominal Mn concentrations $0 \leq x \leq 1$ were prepared by a vapour phase chemical transport technique in an evacuated and sealed quartz tube of 20 cm length and 2 cm diameter. The best single crystals were obtained using AlCl_3 for high Mn concentration compounds ($x > 0.5$)[12] and I_2 for low Mn concentration ($x < 0.5$)[13, 14] as transporting agents in the reaction. About 5 mg/cm^3 of AlCl_3 (4 mg/cm^3 I_2) was added into the ampoules together with 1.5 g of reactants. The starting materials for the growth were polycrystalline samples prepared in a vertical furnace at 1000°C .

The transport reaction was carried out in a two temperature zone furnace in temperature gradients between 900 and 950°C for AlCl_3 and between 800 and 850°C for I_2 . The temperatures were ramped up at 100°C per day. The reaction periods were two or three days, after which the temperature was lowered during a period of about five days. The resulting crystals were layered, had black and bright faces and were very flexible. Their dimensions were up to 1 cm^2 , with thicknesses between 20 and $30 \text{ }\mu\text{m}$.

The resulting Mn concentrations, x , were obtained from the Curie constant, extracted from high temperature magnetic susceptibility measurements. Their precision was around 5%, but the method assumes stoichiometric amounts of the other elements. Additional composition analysis of the crystals was carried out with a Shimadzu EDX-900 energy dispersive X-Ray fluorescence spectrometer. The assumed stoichiometry and the Mn concentrations obtained from magnetic measurements were confirmed within 10%.

2.2. X-Ray measurements

X-Ray Powder Diffraction (XRPD) patterns of the powdered samples were recorded using a Rigaku powder diffractometer utilizing Ni-filtered Cu-K_α radiation (20 mA, 40 kV) $\lambda=1.5418 \text{ \AA}$ in step scanning mode ($0.05^\circ/10 \text{ s}$). Data collection was done for 2θ between 10 and 80 degrees.

Single crystal Laue diagrams were registered using Cu radiation (20 mA, 40 kV), in transmission mode, recorded on an image plate ($100 \text{ mm} \times 86 \text{ mm}$) with imaging distance of 30 mm from the crystal. The exposition time was 30 minutes.

3. Results and discussion

3.1. XRPD profiles

Figure 1 shows the experimental XRPD profiles for all the samples studied. Peaks for the pure MnIn_2Se_4 ($x=1$) and $x=0.87$ samples, as well as for the ZnIn_2Se_4 with $x=0.01$ and $x=0.25$ samples could be indexed assuming the expected crystal structures described in the introduction. For the intermediate concentration samples, peaks from both structures could be discerned, from which we infer a two-phase mixture. In what follows, we will refer to the MnIn_2Se_4 structure as the “rhombohedral” phase, and the ZnIn_2Se_4 structure as the “tetragonal” phase.

Starting from $x=1$ (MnIn_2Se_4), a substitution of 13% of the Mn ions by Zn ions ($x=0.87$) results in the disappearance of reflections from some crystallographic directions, while only the strongest reflections are observed. Assuming the rhombohedral structure is not completely destroyed, the surviving reflections are mostly due to the hexagonal planes, perpendicular to the c -direction of the unit cell. Since the Laue-diagram (see below) still indicates a rhombohedral symmetry, we believe that at this concentration we can still speak of a solid solution, albeit with a decrease of the long range order in the structure.

The substitution with $x=0.67$ leads to an even more drastic reduction of the number and intensities of the peaks, and to a broadening of the profiles. This observation indicates that, at this concentration, the presence of zinc affects the crystallization of the compound even more. This is the least crystalline of the samples we have investigated. Zinc substituting Mn in the rhombohedral phase causes strains in the crystal network, which can lead to broaden reflections. Furthermore, one observes that signs of the presence of a tetragonal phase begin to appear. In Figure 1, the peaks corresponding to the tetragonal and rhombohedral phases are labelled, respectively, “t” and “r” above each observed reflection. We suggest that in this sample the Zn concentration has reached its limit of solubility in the rhombohedral phase, and that the tetragonal phase begins to segregate.

However, the $x=0.60$ sample becomes more crystalline, as one can verify by the narrower peaks and their higher intensities. More reflections due to the tetragonal phase begin to emerge, and we now have clearly a two-phase system. This process is continued with the $x=0.35$ sample, where one can notice the presence of narrow and intense reflections corresponding to both the rhombohedral and the tetragonal phases. This sample is more crystalline than that with $x=0.60$, but now, one can infer the segregation of the rhombohedral phase in a predominantly tetragonal phase, since the sample is richer in Zn atoms. When the Zn concentration increases to 75% ($x=0.25$), only the tetragonal phase is observed in the diffraction profiles. One can suppose that the Mn atoms are in solid solution within the tetragonal phase. Finally, the crystal rich in zinc ($x=0.01$) presents all the peaks expected for the ZnIn_2Se_4 compound [8].

3.2. Lattice parameters

The XRPD patterns allowed the determination of the lattice parameters. They were determined using single reflection peaks, when possible, and pairs of peaks identified for each sample[15]. The averages and error bars were calculated. The results are shown in Table 1, together with literature data for comparison.

For the samples with an average Mn concentration $x \geq 0.35$, which contain the rhombohedral phase, the parameter a does not change considering the error bars. On

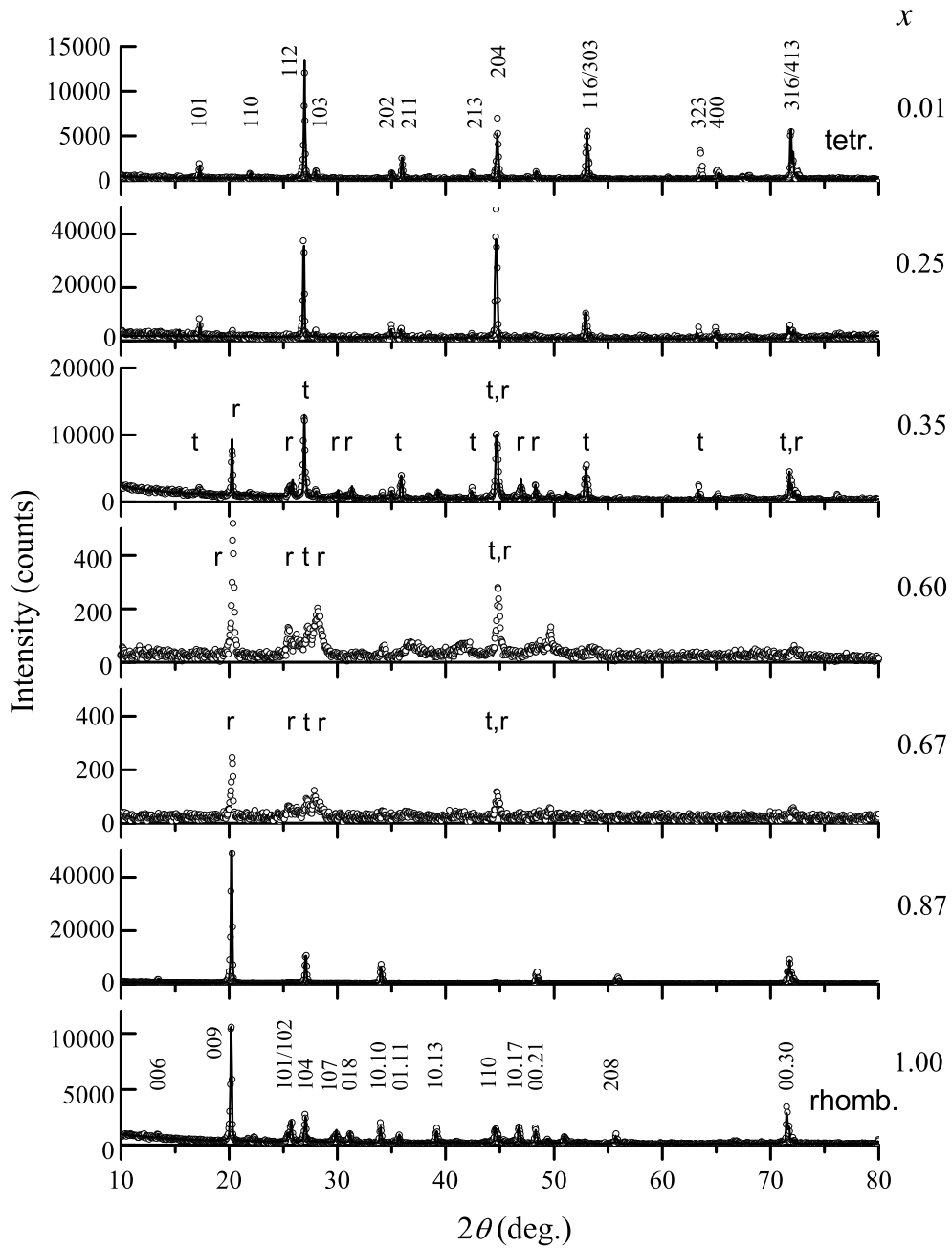


Figure 1. Experimental XRPD profiles (circles) for the $\text{Zn}_{1-x}\text{Mn}_x\text{In}_2\text{Se}_4$ samples. The continuous lines show the results of Rietveld simulations. Also given are Miller indices for the peaks in the tetragonal (t) ($x = 0.01$) and rhombohedral (r) ($x = 1$) phases. For the two-phase samples the identified peaks from each structure are indicated.

Table 1. The lattice parameters obtained for each observed phase in $\text{Zn}_{1-x}\text{Mn}_x\text{In}_2\text{Se}_4$. For the rhombohedral phase, a and c refer to a hexagonal unit cell. For comparison, literature standards are also listed.

x (%)	crystalline phase			
	tetragonal		rhombohedral	
	a (Å)	c (Å)	a (Å)	c (Å)
0 (standard)*	5.710 ± 0.001	11.420 ± 0.002		
1	5.719 ± 0.014	11.514 ± 0.048		
25	5.736 ± 0.009	11.517 ± 0.042		
35	5.729 ± 0.006	11.489 ± 0.023	4.044 ± 0.009	39.444 ± 0.008
60	5.694 ± 0.015	11.418 ± 0.096	4.064 ± 0.015	39.275 ± 0.078
67				39.417 ± 0.037
87			4.046 ± 0.025	39.521 ± 0.026
100			4.046 ± 0.022	39.555 ± 0.034
100 (standard)**			4.051 ± 0.001	39.464 ± 0.002

* (ZnIn_2Se_4 , ICSD collection code 256470)

** (MnIn_2Se_4 , ICSD collection code 69696)

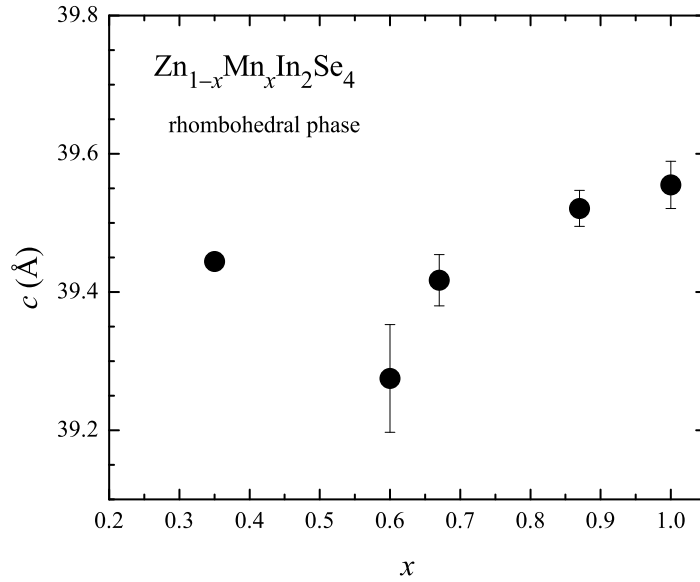


Figure 2. Cell parameter c of the rhombohedral phase for samples with $x \geq 0.35$. The decrease of c for x from 1 down to 0.60 is due to the smaller ionic radius of Zn^{2+} compared to Mn^{2+} .

the other hand, the parameter c decreases with the decrease of Mn concentration down to $x=0.60$ (See Figure 2). The decrease of the c parameter can be associated with the substitution of Mn atoms in the rhombohedral structure by Zn atoms, since the ionic radius of zinc is smaller than that of manganese. For the even higher dilution $x=0.35$, the c parameter increases. We interpret this fact as due to the segregation of the more stable tetragonal phase, leaving a smaller amount of Zn atoms to go into the rhombohedral phase. The cell parameters obtained for the tetragonal phase for x ranging from 0.35 to 0.01 are practically constant considering the uncertainties.

The XRPD profiles were compared with Rietveld simulations using the program PowderCell v2.4 [16]. In the simulations the previously obtained lattice parameters were introduced as constants. The simulation procedure was carried out considering the crystallites in the shape of plates and preferential directions [112] and [001], respectively, for the tetragonal and rhombohedral phases. The results are shown in Figure 1 as continuous lines over the experimental data points. The results are in good agreement with the experimental data, indicating the consistency of the interpretation.

3.3. Laue Patterns

To further evaluate the phase transformation and the crystal quality we measured Laue diagrams for the samples. It was possible to collect the Laue patterns of the samples with $x=1, 0.87, 0.67$ and 0.25 , which sizes were bigger than the cross-section of the X-ray beam. The images were treated using OrientExpress 3.3[17]. The lattice parameters given in Table 1 were introduced in the data input files for the simulations. The method used, based on the indexing of a small set of selected reflections, proposes one or a small number of solutions. The program computes and displays the corresponding simulated Laue patterns (all reflections) or set of patterns. The best solution is easily and unambiguously obtained through the visual comparison of the experimental pattern with the set of simulated ones. Once the correct solution is found, the program makes it possible to compute the rotations which, applied to the sample holder axes, will set the crystal to any desired new orientation. The experimental images are displayed in Figure 3. For comparison, the simulated Laue patterns and the indexes of some reflecting planes are superposed over each image.

The $x=1$ sample (MnIn_2Se_4) presents the rhombohedral structure and the data indicate that the crystal was grown towards the c -axis, the preferential direction observed by XRPD. The good agreement between the experimental and the simulated Laue patterns points to a good crystal quality.

Consistent with our interpretation of the XRPD pattern, the sample with $x=0.87$ also exhibits the rhombohedral structure. However, this sample presents double reflections, which are rotated by $\phi \simeq 12^\circ$ around the beam direction. This fact can be associated with rotated planes (around the c -axis), probably caused by distortions induced by zinc atoms substituting the manganese atoms in the structure.

The Laue diagram of the sample with $x=0.67$ again shows the symmetry expected for the rhombohedral phase and confirms the interpretation of the XRPD data. However, the observed Laue pattern cannot be reproduced by using a single orientation of the crystal. For the displayed simulated pattern, the c -axis was considered as the direction of the X-ray beam. The experimental pattern can be simulated as the superposition of several crystals, each with a different orientation for the c -axis. The relative tilting of different crystals was up to about 9° . This observation points to a distortion of the rhombohedral crystal structure along this axis in agreement with the line broadening observed by XRPD[18, 19]. Simulations considering the presence of the tetragonal phase (as detected in the XRPD spectrum) were made, but no signs of such a phase were seen in the experimental Laue image. Apparently the minority tetragonal phase segregates in a rhombohedral matrix, in the form of small crystallites. They are not oriented coherently enough to form a Laue image.

For the sample with $x=0.25$ the Laue pattern shows only the tetragonal structure and the simulation indicates that the crystal grew along the [112] crystallographic direction. Accordingly, the XRPD presents a more intense peak for this direction.

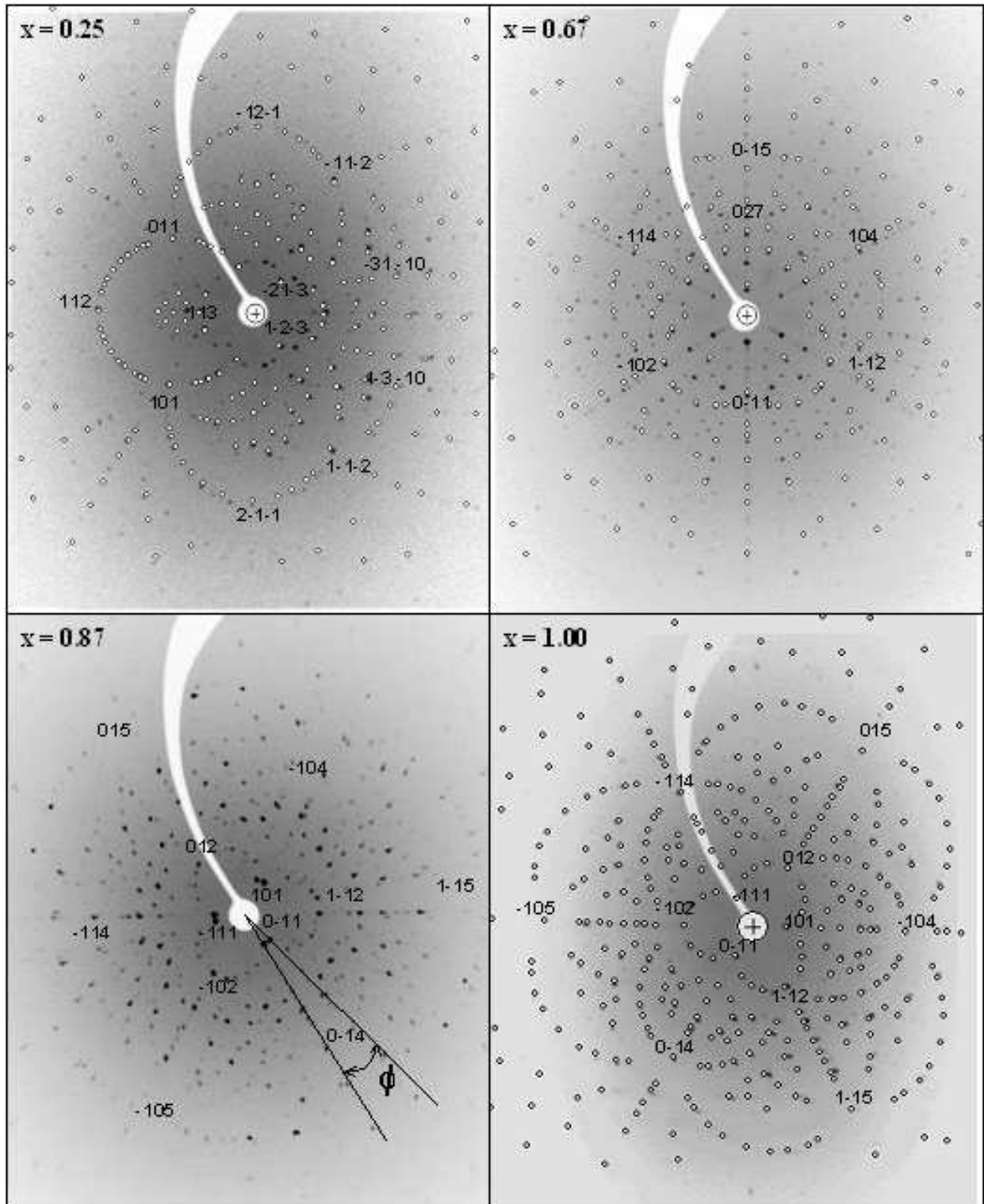


Figure 3. Laue diagrams for the samples with $x = 1, 0.87, 0.67$ and 0.25 . White circles on the pictures for $x = 0.25, 0.67$ and 1.00 represent the OrientExpress simulations.

The (112) crystal plane was oriented perpendicular to the X-ray beam to obtain the Laue diagram for this sample.

4. Conclusions

X-ray diffraction measurements were performed on CVT grown crystals of $\text{Zn}_{1-x}\text{Mn}_x\text{In}_2\text{Se}_4$, with x ranging from 0.01 to 1. The results indicate that the crystals present a purely rhombohedral phase for $x \geq 0.87$ and a purely tetragonal phase for $x \leq 0.25$. For the samples with x between 0.67 and 0.35, a mixture of rhombohedral and tetragonal phases was observed. These results represent approximate limits on the range of concentrations for which single phase solid solutions can be grown. Furthermore, substitution of even small amounts of Mn ($x=0.25$) or Zn ($x=0.87$) leads to a distortion of the original structures and degraded crystallinity.

Acknowledgments

The authors thank M. C. Fantini for helpful discussions. This work was supported in part by the Brazilian agencies CNPq and FAPESP.

References

- [1] Dietl T 1994 *Handbook on Semiconductors* vol 3b ed T S Moss (Amsterdam: North-Holland) p 1251
- [2] Nikiforov K G 1999 *Progr. Crystal Growth and Charact.* **39** 1
- [3] Woolley J C *et al* 1995 *J. Magn. Magn. Mater.* **150** 353
- [4] Morón M C and Hull S 2001 *Phys. Rev. B* **64** 220402
- [5] Goya G F and Sagredo V 2001 *Phys. Rev. B* **64** 235208
- [6] Mantilla J C *et al* 2004 *J. Magn. Magn. Mater.* **272-276P2** 1308
- [7] Shapira Y and Bindilatti V 2002 *J. Appl. Phys.* **92** 4155
- [8] Fiorani D *et al* 1983 *Solid State Commun.* **48** 865
- [9] Gastaldi L *et al* 1987 *J. Solid State Chem.* **66** 251
- [10] Marsh R E and Robinson W R 1988 *J. Solid State Chem.* **73** 591
- [11] Range K-J *et al* 1991 *Z. Naturforsch. B* **46** 1122
- [12] Döll G *et al* 1990 *J. Cryst. Growth* **104** 593
- [13] Sagredo V *et al* 1998 *Inst. Phys. Conf. Ser.* **152** 861
- [14] Schäfer H, 1964 *Chemical Transport Reactions* Academic Press (London)
- [15] J S Kasper and K Lonsdale, editors 1972 *International Tables for X-Ray Crystallography* vol II - Mathematical Tables (Birmingham, England: The Kynoch Press) p 225
- [16] Kraus W and Nolze G 1998 *Powder Diffr.* **13** 256
- [17] Laugier J and Bochu B ORIENTEXPRESS (<http://www.inpg.fr/LMGP>)
- [18] Warren B E and Averbach B L 1950 *J. Appl. Phys.* **21** 595
- [19] Harrison J W 1965 *Acta Cryst.* **20** 390